Available online at www.sciencedirect.com
ScienceDirect
Journal of Sound and Vibration 312 (2008) 234–256
JOURNAL OF SOUND AND VIBRATION
www.elsevier.com/locate/jsvi

Dynamics of a strongly nonlinear vibration absorber coupled to a harmonically excited two-degree-of-freedom system

Y. Starosvetsky, O.V. Gendelman*

Faculty of Mechanical Engineering, Technion—Israel Institute of Technology, Technion City, Haifa 32000, Israel

Received 5 March 2007; received in revised form 10 October 2007; accepted 22 October 2007

Abstract

This paper investigates suppression of vibrations in 2dof forced linear system with a nonlinear energy sink (NES) attached. Ability of the properly tuned single NES to successfully absorb energy from both excited modes of the linear subsystem is demonstrated. The proposed methodology of the NES tuning is based on the results of analytic treatment. The strongly nonlinear vibration absorber is compared to the best-tuned linear one and excitation zones of preference of the nonlinear absorber are revealed.

1. Introduction

The most popular solution in a vibration isolation design is a linear vibration absorber. This solution is based on the additional linear degree-of-freedom (dof) attachment to the existing linear or weakly nonlinear system for the purpose of attenuating vibration over relatively narrow frequency range. This range is centered at the natural frequency of the absorber [1–3]. Effective bandwidth is governed by the damping in the absorber, and a trade-off exists between attenuation efficiency and bandwidth. The problem of a tuned linear vibration absorber coupled to a multi-degree-of-freedom (mdof) primary linear system has been studied extensively in Refs. [4–6].

The linear absorber poses problems when the excitation frequency is not fixed [7], and the frequency response in the neighborhood of existing structural resonances can be adversely affected by the absorber to the extent that the resonant peaks can become very steep [7]. Weakly nonlinear absorbers were proposed for the cases of alternating excitation frequency. They turned out to be effective for somewhat wider frequency range than the linear absorbers [7–11].

Systems comprised of linear substructures with essentially nonlinear attachments are also intensively studied from the viewpoint of the vibration mitigation. Irreversible transient transfer (pumping) of energy from the substructure to the essentially nonlinear attachment was demonstrated and studied in Refs. [12–15]. In the same papers it has been shown that properly designed, essentially nonlinear local attachments may passively absorb energy from transiently loaded linear subsystems, acting as *nonlinear energy sinks* (*NESs*).

*Corresponding author. Tel.: +972 4 8293877; fax: +972 4 8295711.
E-mail address: ovgend@tx.technion.ac.il (O.V. Gendelman).

0022-460X/$ - see front matter © 2007 Elsevier Ltd. All rights reserved.
doi:10.1016/j.jsv.2007.10.035

Addition of a relatively small and spatially localized nonlinear attachment leads to an essential change in the properties of the whole system. Unlike common linear and weakly nonlinear systems, systems with strongly nonlinear elements are able to react efficiently on the amplitude characteristics of the external forcing in a wide range of frequencies [15,16].

It was demonstrated [13,14] that the possibility of the energy pumping phenomenon in non-conservative systems can be understood and explained by studying the energy dependence of the nonlinear un-damped free periodic solutions (nonlinear normal modes (NNM)) of the corresponding conservative system which are obtained when all damping forces are eliminated. Recent investigation [17] based on the approach of invariant manifolds [18,19] has introduced an asymptotic procedure suitable for explicit inclusion of damping within the framework of NNMs.

The steady-state response of the single degree-of-freedom (sdof) linear system with strongly nonlinear attachment to external forcing loading was studied in paper [20]. It was shown theoretically and experimentally that, in spite of weak coupling an essentially nonlinear attachment is capable of absorbing steady-state vibration energy from the linear oscillator, thus localizing the energy away from the directly forced subsystem. The energy absorption by strongly nonlinear attachment is realized over a relatively broad frequency range, making it effective over a range of frequencies.

In recent studies it was demonstrated [21,22] that in close vicinity of the main resonance the system with NES can exhibit quasi-periodic rather than simple periodic response, leading to qualitatively different dynamical behavior. As it was shown in paper [22], strong mass asymmetry in periodically forced systems with essential nonlinearity may cause response regime qualitatively different from either simply periodic or weakly modulated regimes in the vicinity of 1:1 resonance. This regime is characterized by very deep oscillations of the modulated amplitude comparable to the amplitude of the response itself. This response regime was considered in papers [22,23] and referred to as strongly quasi-periodic response (SQR). In fact, as it was demonstrated in Ref. [23] such response may be also phase locked or chaotic. In order to emphasize the difference of the response from simply periodic and weakly modulated quasi-periodic response we use the term "strongly modulated response" (SMR). In the same paper [23], novel analytic approach was proposed for the SMR description.

Possible effectiveness of the SMR for vibration absorption and mitigation compared to the best-tuned linear vibration absorber was demonstrated in Ref. [24]. Extension of the system studied in Refs. [22–24] by frequency detuning parameter inclusion in the analysis was carried out in Refs. [29,30]. Novel tools for prediction of the SMR in the extended system via one-dimensional (1D) maps were described in Ref. [30].

Recently the efficiency of the NES in vibration suppression and mitigation has obtained additional experimental approval. In paper [29] the effects of energy pumping with transient forcing and strongly nonlinear coupling were verified experimentally. In paper [31] the NES was efficiently used for suppression of the aeroelastic instability. Experimental evidence of the energy pumping in acoustics is described in Ref. [32].

The results mentioned above have motivated us to extend the analytic and numeric treatment developed in Refs. [22–24,29–30] to a harmonically excited 3dof system (including NES attached). Thus, we investigate the performance of essentially nonlinear vibration absorber attached to forced mdof linear primary system.

The structure of the paper is as follows. The second section is devoted to model description. Section 3 brings an analytical treatment including periodic regimes and SMR description. Section 4 is fully based on the analytic treatment developed in Section 3 and provides NES tuning guidelines. Section 5 contains numerical verifications of the analytical model and also studies effectiveness of the NES compared to the linear vibrations absorber. Section 6 contains concluding remarks and discussion.

2. Description of the model

The system considered in the present paper consists of harmonically excited 2dof system of linear coupled oscillators (with identical masses) and NES attached to it. By the term NES we mean a small mass (relative to the linear oscillator mass) attached via essentially nonlinear spring (pure cubic nonlinearity) and linear viscous damper to the linear subsystem as it is illustrated in Fig. 1.

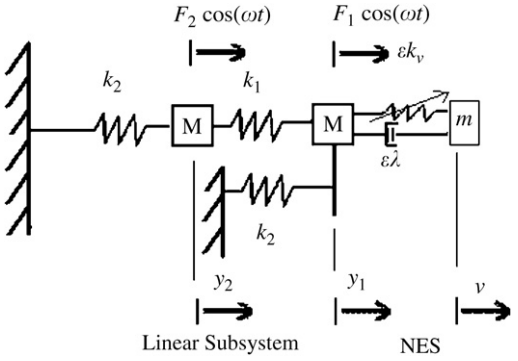

Fig. 1. Mechanical model of the system.

As it was mentioned above masses of linear oscillators are identical and therefore may be taken as unity without loss of generality ($M = 1$). The system is described by the following equations:

$$\begin{aligned}
&\ddot{y}_2 + k_2 y_2 + k_1(y_2 - y_1) = \varepsilon F_2 \cos(\omega t),\\
&\ddot{y}_1 + k_2 y_1 + k_1(y_1 - y_2) + \varepsilon k_v (y_1 - v)^3 + \varepsilon\lambda(\dot{y}_1 - \dot{v}) = \varepsilon F_1 \cos(\omega t),\\
&\varepsilon\ddot{v} + \varepsilon k_v (v - y_1)^3 + \varepsilon\lambda(\dot{v} - \dot{y}_1) = 0,
\end{aligned} \tag{1}$$

where y_1, y_2, v are the displacements of the linear oscillators and NES, respectively, $\varepsilon\lambda$ is the damping coefficient, εF_i $(i = 1, 2)$ are the amplitudes of excitation of each linear oscillator. $\varepsilon \ll 1$ is a small parameter which establishes the order of magnitude for external excitation, damping, coupling and mass of the NES which is adopted to be ε ($m = \varepsilon$). Eq. (1) may be rescaled in the following way:

$$\begin{aligned}
&t = \sqrt{k_1}\tau,\ \frac{\mathrm{d}}{\mathrm{d}t} = \sqrt{k_1}\frac{\mathrm{d}}{\mathrm{d}\tau},\ \tilde{k}_2 = \frac{k_2}{k_1},\\
&\tilde{\lambda} = \frac{\lambda}{\sqrt{k_1}},\ \tilde{F}_1 = \frac{F_1}{k_1},\ \tilde{F}_2 = \frac{F_2}{k_1},\ \tilde{k}_v = \frac{k_v}{k_1}.
\end{aligned} \tag{2}$$

Substitution of Eq. (2) into Eq. (1) yields

$$\begin{aligned}
&y_2'' + (\tilde{k}_2 + 1)y_2 - y_1 = \varepsilon\tilde{F}_2 \cos(\omega t),\\
&y_1'' + (\tilde{k}_2 + 1)y_1 - y_2 = \varepsilon\tilde{F}_1 \cos(\omega t) - \varepsilon\tilde{k}_v (y_1 - v)^3 - \varepsilon\tilde{\lambda}(y_1' - v'),\\
&\varepsilon v'' + \varepsilon\tilde{k}_v (v - y_1)^3 + \varepsilon\tilde{\lambda}(v' - y_1') = 0,
\end{aligned} \tag{3}$$

where prime denotes the differentiation with respect to τ. Two natural frequencies of the linear oscillators are assumed to be of the same order of magnitude, incommensurate and remote (distance between dimensionless frequencies is of order $O(1)$). Therefore the value of spring stiffness $\tilde{k}_2$ was chosen in a way to provide two distinct incommensurate natural frequencies—of course, it is the most generic case, since any significant internal resonance should be treated as exceptional situation. Thus, taking $\tilde{k}_2 = 1$ one obtains the following natural frequencies$\omega_2 = \sqrt{3}$, $\omega_1 = 1$. Such choice may seem rather restrictive, but from the following development it will be clear that the particular values of the frequencies are of no significance for analytic procedure proposed. The only significant physical condition is an absence of internal resonances in the linear subsystem.

Modal coordinates are introduced according to following relationship:

$$\begin{aligned}
&y_1 = \frac{1}{\sqrt{2}}(x_1 + x_2),\\
&y_2 = \frac{1}{\sqrt{2}}(x_1 - x_2),
\end{aligned} \tag{4}$$

Transformation of Eq. (3) to modal coordinates yields

$$\begin{aligned}
x_2'' + 3x_2 &= -\frac{\varepsilon\tilde{A}_2}{\sqrt{2}}\cos(\omega t) - \frac{\varepsilon\tilde{k}_v}{\sqrt{2}}\left(\frac{(x_1+x_2)}{\sqrt{2}} - v\right)^3 - \frac{\varepsilon\tilde{\lambda}}{\sqrt{2}}\left(\frac{(x_1'+x_2')}{\sqrt{2}} - v'\right),\\
x_1'' + x_1 &= \frac{\varepsilon\tilde{A}_1}{\sqrt{2}}\cos(\omega t) - \frac{\varepsilon\tilde{k}_v}{\sqrt{2}}\left(\frac{(x_1+x_2)}{\sqrt{2}} - v\right)^3 - \frac{\varepsilon\tilde{\lambda}}{\sqrt{2}}\left(\frac{(x_1'+x_2')}{\sqrt{2}} - v'\right),\\
\varepsilon v'' &+ \varepsilon\tilde{k}_v\left(v - \frac{(x_1+x_2)}{\sqrt{2}}\right)^3 + \varepsilon\tilde{\lambda}\left(v' - \frac{0(x_1'+x_2')}{\sqrt{2}}\right) = 0,
\end{aligned} \tag{5}$$

where $\tilde{A}_1 = \tilde{F}_1 + \tilde{F}_2$, $\tilde{A}_2 = \tilde{F}_1 - \tilde{F}_2$.

Additional rescaling is performed as follows:

$$\tilde{x}_1 = \frac{x_1}{\sqrt{2}},\ \tilde{x}_2 = \frac{x_2}{\sqrt{2}},\ \tilde{\varepsilon} = \frac{\varepsilon}{2}. \tag{6}$$

New coordinates are substituted into Eq. (5), this brings the system to more convenient form:

$$\begin{aligned}
\tilde{x}_2'' + 3\tilde{x}_2 &= -\tilde{\varepsilon}\tilde{A}_2\cos(\omega t) - \tilde{\varepsilon}\tilde{k}_v(\tilde{x}_1 + \tilde{x}_2 - v)^3 - \tilde{\varepsilon}\tilde{\lambda}(\tilde{x}_1' + \tilde{x}_2' - v'),\\
\tilde{x}_1'' + \tilde{x}_1 &= \tilde{\varepsilon}\tilde{A}_1\cos(\omega t) - \tilde{\varepsilon}\tilde{k}_v(\tilde{x}_1 + \tilde{x}_2 - v)^3 - \tilde{\varepsilon}\tilde{\lambda}(\tilde{x}_1' + \tilde{x}_2' - v'),\\
\tilde{\varepsilon}v'' &+ \tilde{\varepsilon}\tilde{k}_v(v - \tilde{x}_1 + \tilde{x}_2)^3 + \tilde{\varepsilon}\tilde{\lambda}(v' - \tilde{x}_1' + \tilde{x}_2') = 0,
\end{aligned} \tag{7}$$

For the sake of convenience 'tilde' will be dropped in further expressions.

3. Analytic treatment

The present subsection is fully devoted to the analytical study of the periodic regimes and SMR in the vicinity of two most dangerous resonances, where the frequency of the external excitation is close to 1 or $\sqrt{3}$ (modal natural frequencies of linear subsystem).

3.1. Periodic regimes

Periodic regimes are sought using complex-averaging method. Before we proceed with direct calculation of the periodic responses it is convenient to perform additional algebraic manipulation. Thus leaving the first two equations of Eq. (7) unchanged we derive the third equation by adding the first two equations of Eq. (7) and subtracting from the sum the third equation of Eq. (7). Defining new variable as follows:

$$x_1 + x_2 - v \to w, \tag{8}$$

system (7) is rewritten in the more convenient form:

$$\begin{aligned}
x_2'' + 3x_2 &= -\varepsilon A_2\cos(\omega t) - \varepsilon k_v w^3 - \varepsilon\lambda w',\\
x_1'' + x_1 &= \varepsilon A_1\cos(\omega t) - \varepsilon k_v w^3 - \varepsilon\lambda w',\\
w'' + 3x_2 + x_1 &= \varepsilon(A_1 - A_2)\cos(\omega t) - (1+2\varepsilon)k_v w^3 - (1+2\varepsilon)\lambda w'.
\end{aligned} \tag{9}$$

We begin our treatment from the excitation in the vicinity of the first mode. Thus, an excitation frequency is detuned off in the following form:

$$\omega = 1 + \varepsilon\sigma. \tag{10}$$

Complex variables are introduced as follows:

$$\begin{aligned}
x_1' + \mathrm{i}x_1 &= \varphi_1\exp(\mathrm{i}\tau),\\
x_2' + \mathrm{i}x_2 &= \varphi_2\exp(\mathrm{i}\tau),\\
w' + \mathrm{i}w &= \varphi_w\exp(\mathrm{i}\tau),
\end{aligned} \tag{11}$$

where φ_1, φ_2, φ_w are assumed as slowly evolving compared to the frequency of external excitation.

Introducing Eqs. (10) and (11) into Eq. (9) and averaging over one period of the external excitation we obtain the following system of slow modulation:

$$\begin{aligned}
\varphi_2' - \mathrm{i}\varphi_2 &= \frac{-\varepsilon A_2}{2}\exp(\mathrm{i}\varepsilon\sigma\tau) + \frac{3\varepsilon}{8}\mathrm{i}k_v|\varphi_w|^2\varphi_w - \frac{\varepsilon\lambda}{2}\varphi_w,\\
\varphi_1' &= \frac{\varepsilon A_1}{2}\exp(\mathrm{i}\varepsilon\sigma\tau) + \frac{3\varepsilon}{8}\mathrm{i}k_v|\varphi_w|^2\varphi_w - \frac{\varepsilon\lambda}{2}\varphi_w,\\
\varphi_w' + \frac{\mathrm{i}}{2}\varphi_w - \frac{3\mathrm{i}}{2}\varphi_2 - \frac{\mathrm{i}}{2}\varphi_1 &= \frac{\varepsilon(A_1 - A_2)}{2}\exp(\mathrm{i}\varepsilon\sigma\tau)\\
&\quad + (1+2\varepsilon)\frac{3}{8}\mathrm{i}k_v|\varphi_w|^2\varphi_w - (1+2\varepsilon)\frac{\lambda}{2}\varphi_w.
\end{aligned} \tag{12}$$

As one can note, system obtained in Eq. (12) is not autonomous then additional change of variables should be applied in order to reduce the system into the autonomous one.

Complex variable φ_i may be written in general form:

$$\varphi_i = N_i\exp(\mathrm{i}\theta_i). \tag{13}$$

New phase coordinate is introduced:

$$\gamma_i = \theta_i - \varepsilon\sigma t. \tag{14}$$

By substituting Eq. (14) into Eq. (13) and performing simple algebraic manipulations, Eq. (12) are reduced to the autonomous form:

$$\begin{aligned}
\dot\varphi_2 + \mathrm{i}(\varepsilon\sigma - 1)\varphi_2 &= \frac{-\varepsilon A_2}{2} + \frac{3\varepsilon}{8}\mathrm{i}k_v|\varphi_w|^2\varphi_w - \frac{\varepsilon\lambda}{2}\varphi_w,\\
\varphi_1 + \mathrm{i}\varepsilon\sigma\varphi_1 &= \frac{\varepsilon A_1}{2} + \frac{3\varepsilon}{8}\mathrm{i}k_v|\varphi_w|^2\varphi_w - \frac{\varepsilon\lambda}{2}\varphi_w,\\
\dot\varphi_w + \mathrm{i}\left(\frac{1}{2} + \varepsilon\sigma\right)\varphi_w - \frac{3\mathrm{i}}{2}\varphi_2 - \frac{\mathrm{i}}{2}\varphi_1 &= \frac{\varepsilon(A_1 - A_2)}{2}\\
&\quad + (1+2\varepsilon)\frac{3}{8}\mathrm{i}k_v|\varphi_w|^2\varphi_w - (1+2\varepsilon)\frac{\lambda}{2}\varphi_w.
\end{aligned} \tag{15}$$

In order to compute the periodic response regimes of the system we seek for the fixed points of Eq. (15). Thus, setting ($\dot\varphi_1 = \dot\varphi_2 = \dot\varphi_w = 0$) we obtain a system of algebraic equations:

$$\begin{aligned}
\mathrm{i}(\varepsilon\sigma - 1)\varphi_{20} &= \frac{-\varepsilon A_2}{2} + \frac{3\varepsilon}{8}\mathrm{i}k_v|\varphi_{w0}|^2\varphi_{w0} - \frac{\varepsilon\lambda}{2}\varphi_{w0},\\
\mathrm{i}\varepsilon\sigma\varphi_{10} &= \frac{\varepsilon A_1}{2} + \frac{3\varepsilon}{8}\mathrm{i}k_v|\varphi_{w0}|^2\varphi_{w0} - \frac{\varepsilon\lambda}{2}\varphi_{w0},\\
\mathrm{i}\left(\frac{1}{2} + \varepsilon\sigma\right)\varphi_{w0} - \frac{3\mathrm{i}}{2}\varphi_{20} - \frac{\mathrm{i}}{2}\varphi_{10} &= \frac{\varepsilon(A_1 - A_2)}{2}\\
&\quad + (1+2\varepsilon)\frac{3}{8}\mathrm{i}k_v|\varphi_{w0}|^2\varphi_{w0} - (1+2\varepsilon)\frac{\lambda}{2}\varphi_{w0}.
\end{aligned} \tag{16}$$

Solutions of Eq. (16) refer to the periodic regimes and are easily calculated by simple algebraic manipulations:

$$\begin{aligned}
\alpha_2\bar\alpha_2|\varphi_{w0}|^6 + (\alpha_2\bar\alpha_1 + \alpha_1\bar\alpha_2)|\varphi_{w0}|^4 + \alpha_1\bar\alpha_1|\varphi_{w0}|^2 &= \alpha_3\bar\alpha_3,\\
\varphi_{w0} &= \frac{-\alpha_3}{\alpha_1 + \alpha_2|\varphi_{w0}|^2},
\end{aligned}$$

$$
\begin{aligned}
\varphi_{20} &= \frac{\mathrm{i}\varepsilon A_2}{2(\varepsilon\sigma-1)} + \frac{3\varepsilon k_v}{8(\varepsilon\sigma-1)}\left|\varphi_{w0}\right|^2\varphi_{w0} + \frac{\mathrm{i}\varepsilon\lambda}{2(\varepsilon\sigma-1)}\varphi_{w0},\\
\varphi_{10} &= -\frac{\mathrm{i}A_1}{2\sigma} + \frac{3}{8\sigma}k_v\left|\varphi_{w0}\right|^2\varphi_{w0} + \frac{\mathrm{i}\lambda}{2\sigma}\varphi_{w0},\\
\alpha_1 &= \mathrm{i}(\varepsilon\sigma+1/2) + \frac{3\varepsilon\lambda}{4(\varepsilon\sigma-1)} + \frac{\lambda}{4\sigma} + (1+2\varepsilon)\frac{\lambda}{2},\\
\alpha_2 &= -\left(\frac{9\mathrm{i}\varepsilon k_v}{16(\varepsilon\sigma-1)} + \frac{3\mathrm{i}k_v}{16\sigma} + \frac{3\mathrm{i}}{8}k_v(1+2\varepsilon)\right),\\
\alpha_3 &= \frac{3\varepsilon A_2}{4(\varepsilon\sigma-1)} - \frac{A_1}{4\sigma} - \frac{\varepsilon(A_1-A_2)}{2}.
\end{aligned}
\tag{17}
$$

Saddle node and Hopf bifurcations were revealed by the stability analysis. They are marked on the frequency response diagram (Fig. 2).

We proceed with an excitation in the vicinity of the second mode. Thus, frequency of excitation is detuned off near the second mode in the following way:

$$\omega = \sqrt{3} + \varepsilon\sigma. \tag{18}$$

In this case it is convenient to rescale the time scale of Eq. (9) with respect to natural frequency of the second mode:

$$\tilde{\tau} = \sqrt{3}\tau. \tag{19}$$

Writing Eq. (9) in terms of new time scale one obtains

$$
\begin{aligned}
x_2'' + x_2 &= -\varepsilon\tilde{A}_2\cos(\omega\tilde{\tau}) - \varepsilon\tilde{k}_v w^3 - \varepsilon\tilde{\lambda}w',\\
x_1'' + \tfrac{1}{3}x_1 &= \varepsilon\tilde{A}_1\cos(\omega\tilde{\tau}) - \varepsilon\tilde{k}_v w^3 - \varepsilon\tilde{\lambda}w',\\
w'' + x_2 + \tfrac{1}{3}x_1 &= \varepsilon(\tilde{A}_1-\tilde{A}_2)\cos(\omega\tilde{\tau}) - (1+2\varepsilon)\tilde{k}_v w^3 - (1+2\varepsilon)\tilde{\lambda}w',
\end{aligned}
\tag{20}
$$

where $\tilde{A}_2 = A_2/3$, $\tilde{A}_1 = A_1/3$, $\tilde{k}_v = k_v/3$, $\tilde{\lambda} = \lambda/\sqrt{3}$, $\tilde{\sigma} = \sigma/\sqrt{3}$. Prime denotes differentiation with respect to $\tilde{\tau}$.

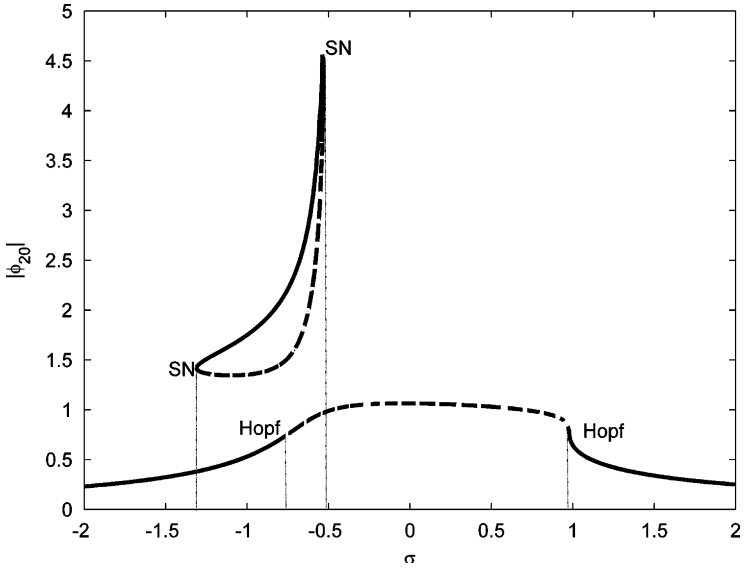

Fig. 2. Thin solid line relates to stable solution and bold solid line relates to unstable ones.

Complex coordinates here are introduced as

$$\begin{aligned} x_1' + \mathrm{i}x_1 &= \varphi_1 \exp(\mathrm{i}\tilde{\tau}),\\ x_2' + \mathrm{i}x_2 &= \varphi_2 \exp(\mathrm{i}\tilde{\tau}),\\ w' + \mathrm{i}w &= \varphi_w \exp(\mathrm{i}\tilde{\tau}). \end{aligned} \tag{21}$$

Introducing Eq. (21) into Eq. (20) and averaging over one time period of external excitation one obtains slow modulated system (the treatment is quite identical to one in the vicinity of the first resonance):

$$\begin{aligned} \varphi_2' + \mathrm{i}\varepsilon\tilde{\sigma}\varphi_2 &= -\frac{\varepsilon\tilde{A}_2}{2} + \frac{3}{8}\mathrm{i}\varepsilon\tilde{k}_v|\varphi_w|^2\varphi_w - \frac{\varepsilon\tilde{\lambda}}{2}\varphi_w,\\ \varphi_1' + \mathrm{i}\left(\varepsilon\tilde{\sigma} + \frac{1}{3}\right)\varphi_1 &= \frac{\varepsilon\tilde{A}_1}{2} + \frac{3}{8}\mathrm{i}\varepsilon\tilde{k}_v|\varphi_w|^2\varphi_w - \frac{\varepsilon\tilde{\lambda}}{2}\varphi_w,\\ \varphi_w' + \mathrm{i}\left(\varepsilon\tilde{\sigma} + \frac{1}{2}\right)\varphi_1 &= \frac{\mathrm{i}}{2}\varphi_2 + \frac{\mathrm{i}}{6}\varphi_1 + \frac{\varepsilon(\tilde{A}_1 - \tilde{A}_2)}{2} + (1+2\varepsilon)\tilde{k}_v\frac{3}{8}\mathrm{i}|\varphi_w|^2\varphi_w - (1+2\varepsilon)\frac{\tilde{\lambda}}{2}\varphi_w. \end{aligned} \tag{22}$$

Fixed points of Eq. (22):

$$\begin{aligned} \alpha_2\bar{\alpha}_2|\varphi_{w0}|^6 + (\alpha_2\bar{\alpha}_1 + \alpha_1\bar{\alpha}_2)|\varphi_{w0}|^4 + \alpha_1\bar{\alpha}_1|\varphi_{w0}|^2 &= \alpha_3\bar{\alpha}_3,\\ \varphi_{w0} &= \frac{-\alpha_3}{\alpha_1 + \alpha_2|\varphi_{w0}|^2},\\ \varphi_{20} &= \frac{\mathrm{i}\tilde{A}_2}{2\tilde{\sigma}} + \frac{3\tilde{k}_v}{8\tilde{\sigma}}|\varphi_{w0}|^2\varphi_{w0} + \frac{\mathrm{i}\tilde{\lambda}}{2\tilde{\sigma}}\varphi_{w0},\\ \varphi_{10} &= -\frac{\mathrm{i}\varepsilon\tilde{A}_1}{2(\varepsilon\tilde{\sigma} + 1/3)} + \frac{3\varepsilon\tilde{k}_v}{8(\varepsilon\tilde{\sigma} + 1/3)}|\varphi_{w0}|^2\varphi_{w0} + \frac{\mathrm{i}\varepsilon\tilde{\lambda}}{2(\varepsilon\tilde{\sigma} + 1/3)}\varphi_{w0},\\ \alpha_1 &= \mathrm{i}(\varepsilon\tilde{\sigma} + 1/2) + \frac{\varepsilon\tilde{\lambda}}{12(\varepsilon\tilde{\sigma} + 1/3)} + \frac{\tilde{\lambda}}{4\tilde{\sigma}} + (1+2\varepsilon)\frac{\tilde{\lambda}}{2},\\ \alpha_2 &= -\mathrm{i}\left(\frac{\varepsilon\tilde{k}_v}{16(\varepsilon\tilde{\sigma} + 1/3)} + \frac{3\tilde{k}_v}{16\tilde{\sigma}} + \frac{3}{8}\tilde{k}_v(1+2\varepsilon)\right),\\ \alpha_3 &= -\frac{\varepsilon(\tilde{A}_1 - \tilde{A}_2)}{2} + \frac{\tilde{A}_2}{4\tilde{\sigma}} - \frac{\varepsilon\tilde{A}_1}{12(\varepsilon\tilde{\sigma} + 1/3)}. \end{aligned} \tag{23}$$

Saddle node and Hopf bifurcations were also revealed in case of second mode excitation by the stability analysis. They are marked on the frequency response diagram (Fig. 3).

By now we have described periodic solutions in the vicinity of each excited mode of the system. In the current paper we do not bring conditions for the local bifurcations of periodic solutions in the space of the system parameters as it was done in Refs. [22,30] due to an awkwardness of calculations (Fig. 4).

3.2. Strongly modulated response description

Strongly modulated regime has been extensively studied in papers [21–24,29]. Analytical study of SMR brought here is fully based on the results of papers [22,23,29]. As in a case of periodic regimes, analytical treatment of SMR will be carried out separately for each excited mode. Thus, we start with an excitation in the vicinity of the first mode. Frequency of excitation is detuned off as it was done in Eq. (10). It is essential to note that by exciting the first mode the magnitude of the second mode will be of order ε since two modal natural frequencies are remote and incommensurate. Let us rewrite system (7) in the following way:

$$\begin{aligned} x_2'' + 3x_2 &= -\varepsilon A_2\cos((1+\varepsilon\sigma)\tau) - \varepsilon k_v(x_1 + \varepsilon x_2 - v)^3 - \varepsilon\lambda\left(x_1' + \varepsilon x_2' - v'\right),\\ x_1'' + x_1 &= \varepsilon A_1\cos((1+\varepsilon\sigma)\tau) - \varepsilon k_v(x_1 + \varepsilon x_2 - v)^3 - \varepsilon\lambda(x_1' + \varepsilon x_2' - v'),\\ v'' + k_v(v - x_1 - \varepsilon x_2)^3 + \lambda(v' - x_1' - \varepsilon x_2') &= 0. \end{aligned} \tag{24}$$

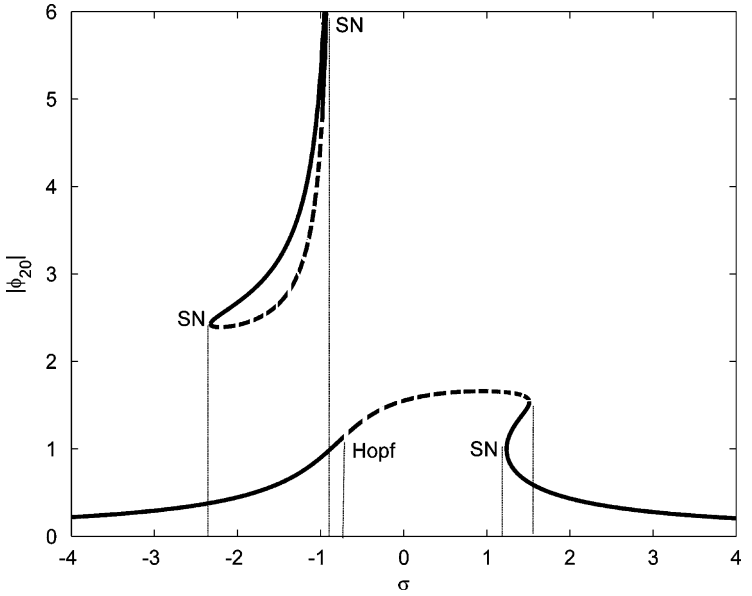

Fig. 3. Thin solid line relates to stable solution and bold solid line relates to unstable one.

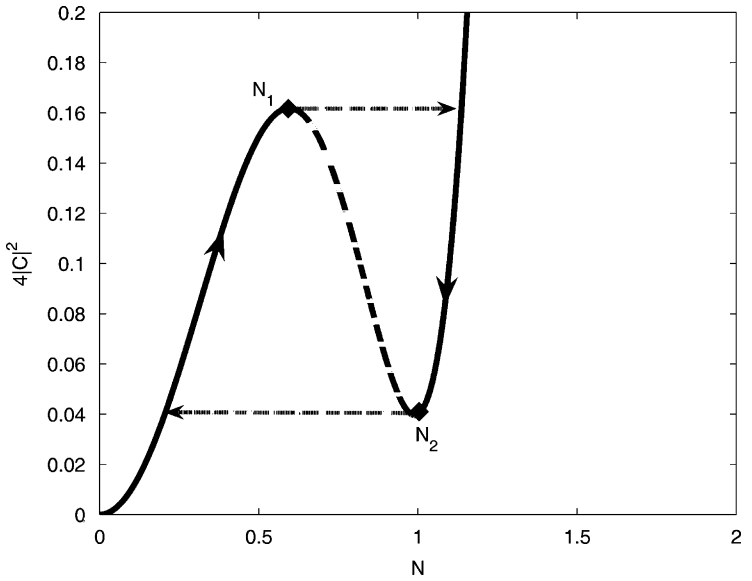

Fig. 4. Projection of the slow invariant manifold of the system in accordance with Eq. (33), $\lambda = 0.2$. The unstable branch is denoted by dashed line. Arrows denote hypothetic jumps in the regime of the relaxation oscillations.

Further analytical treatment of SMR in the vicinity of (1:1) resonance (first mode excitation) concerns only the last two equations. As it will be shown latter the terms which include εx_2 may be omitted in the analysis, then it is convenient to keep it in the equations without change. Following the analysis performed in Ref. [22,23] successive changes of variables are performed:

$$u = x_1 + \varepsilon v,$$
$$w = x_1 - v \tag{25}$$

(transition to coordinates "center of mass—internal displacement") and

$$\varphi_u \exp(\mathrm{i}t) = \dot{u} + \mathrm{i}u,$$
$$\varphi_w \exp(\mathrm{i}t) = \dot{w} + \mathrm{i}w, \tag{26}$$

where complex variables φ_j, $j = 1, 2$ describe slow modulation of variables u and w, respectively, yield the following equations for modulation amplitudes (keeping only the terms up to order $O(\varepsilon)$):

$$\varphi_u' + \mathrm{i}\varepsilon\sigma\varphi_u + \frac{\mathrm{i}\varepsilon}{2(1+\varepsilon)}(\varphi_u - \varphi_w) = \frac{\varepsilon A_1}{2},$$
$$\varphi_w' + \mathrm{i}\varepsilon\sigma\varphi_w + (1+\varepsilon)\frac{\lambda}{2}\varphi_w + \frac{\mathrm{i}}{2(1+\varepsilon)}(\varphi_w - \varphi_u)$$
$$+ k_v(1+\varepsilon)\left(\frac{-3\mathrm{i}(1+\varepsilon)}{8}|\varphi_w|^2\varphi_w + \varepsilon\langle 3w^2 x_2\rangle\right) = \frac{\varepsilon A_1}{2}. \tag{27}$$

Two coupled differential equations of Eq. (27) may be combined into one of the second order:

$$\varphi_w'' + \frac{\mathrm{d}}{\mathrm{d}\tau}\left\{\left(\alpha + \frac{\mathrm{i}\varepsilon}{2(1+\varepsilon)} + \mathrm{i}\varepsilon\sigma\right)\varphi_w + (1+\varepsilon)k_v\left(-\frac{3\mathrm{i}}{8}|\varphi_w|^2\varphi_w + \varepsilon\langle 3w^2 x_2\rangle\right)\right\}$$
$$+ \frac{\mathrm{i}\varepsilon}{2(1+\varepsilon)}(1+2\sigma)\left\{\alpha\varphi_w + k_v\left(-\frac{3\mathrm{i}}{8}|\varphi_w|^2\varphi_w + \varepsilon\langle 3w^2 x_2\rangle\right)\right\} - \frac{\mathrm{i}\varepsilon\beta}{2(1+\varepsilon)}\varphi_w = \frac{\varepsilon A_1\beta}{2}, \tag{28}$$

where

$$\alpha = \frac{\lambda(1+\varepsilon)}{2} + \frac{\mathrm{i}}{2(1+\varepsilon)} + \mathrm{i}\varepsilon\sigma,\ \beta = \frac{\mathrm{i}}{2(1+\varepsilon)}.$$

Multiple scale expansion is introduced as

$$\varphi_w = \varphi_w(\tau_0, \tau_1, \ldots),\ \frac{\mathrm{d}}{\mathrm{d}t} = \frac{\partial}{\partial\tau_0} + \varepsilon\frac{\partial}{\partial\tau_1} + \cdots,$$
$$\tau_k = \varepsilon^k t, k = 0, 1, \ldots\ . \tag{29}$$

Substituting Eq. (29) into Eq. (28) and equating the like powers of ε one obtains equations for zero and the first-order approximations:

$$\varepsilon^0 : \frac{\partial\varphi_w}{\partial\tau_0^2} + \frac{\partial}{\partial\tau_0}\left[\frac{\lambda\varphi_w}{2} + \frac{\mathrm{i}\varphi_w}{2} - \frac{3\mathrm{i}k_v|\varphi_w|^2\varphi_w}{8}\right] = 0,$$
$$\varepsilon^1 : 2\frac{\partial^2\varphi_w}{\partial\tau_0\partial\tau_1} + \frac{\partial}{\partial\tau_1}\left[\frac{\lambda\varphi_w}{2} + \frac{\mathrm{i}\varphi_w}{2} - \frac{3\mathrm{i}k_v|\varphi_w|^2\varphi_w}{8}\right]$$
$$+ \frac{\partial}{\partial\tau_0}\left[\left(\frac{\lambda}{2} + \frac{\mathrm{i}}{2(1+\varepsilon)} + i\sigma\right)\varphi_w + k_v\left(-\frac{3\mathrm{i}}{8}|\varphi_w|^2\varphi_w + \langle 3w^2 x_2\rangle\right)\right]$$
$$+ \frac{\mathrm{i}(1+2\sigma)}{2}\left[\frac{\lambda\varphi_w}{2} + \frac{\mathrm{i}\varphi_w}{2} - \frac{3\mathrm{i}k_v|\varphi_w|^2\varphi_w}{8}\right] - \frac{\mathrm{i}\varphi_w\beta}{2} = \frac{A\beta}{2}. \tag{30}$$

The first equation of Eq. (30) describes "fast" evolution of the averaged system. It can be trivially integrated:

$$\frac{\partial}{\partial\tau_0}\varphi_w + \left(\frac{\mathrm{i}}{2}\varphi_w + \frac{\lambda}{2}\varphi_w - \frac{3\mathrm{i}k_v}{8}|\varphi_w|^2\varphi_w\right) = C(\tau_1, \ldots), \tag{31}$$

where C is arbitrary function of higher order time scales. Approximations of higher orders are not used in current analysis. Then for the sake of brevity only dependence on time scales τ_0 and τ_1 will be denoted

explicitly below. Fixed points $\Phi(\tau_1)$ of Eq. (31) depend only on time scale τ_1 and obey algebraic equation:

$$\frac{\mathrm{i}}{2}\Phi+\frac{\lambda}{2}\Phi-\frac{3\mathrm{i}k_v}{8}|\Phi|^2\Phi=C(\tau_1). \tag{32}$$

Eq. (32) is easily solved by taking $\Phi(\tau_1)=N(\tau_1)\exp(\mathrm{i}\theta(\tau_1))$ and performing trivial calculations:

$$\lambda^2+1-\frac{3k_v}{2}N^4+\frac{9k_v^2}{16}N^6=4\left|C(\tau_1)\right|^2,$$

or, equivalently

$$\begin{aligned}&\lambda^2+1-\frac{3k_v}{2}Z(\tau_1)^2+\frac{9k_v^2}{16}Z(\tau_1)^3=4\left|C(\tau_1)\right|^2,\\&Z(\tau_1)=(N(\tau_1))^2.\end{aligned} \tag{33}$$

Expression for argument of the fixed point may be written as

$$\theta(\tau_1)=\arg\ C(\tau_1)-\tan^{-1}\left(\frac{1-3\mathrm{i}k_v/4Z(\tau_1)^2}{\lambda}\right), \tag{34}$$

where $Z(\tau_1)$ is solution of Eq. (33). Number of solutions of Eq. (10) depends on $|C(\tau_1)|$ and λ. Function in the left-hand side can be monotonous or have maximum and minimum. In the former case the change of $|C(\tau_1)|$ has no effect on the number of solutions—Eq. (10) will have one positive solution. In the latter case the change of $|C(\tau_1)|$ will bring about a pair of saddle–node bifurcations. In order to distinguish between different cases we should check whether the derivative of the left-hand side of Eq. (33) has roots. If they exist, they are expressed as

$$Z^*_{1,2}=\frac{2\pm\sqrt{1-3\lambda^2}}{3}. \tag{35}$$

Therefore two roots and pair of saddle–node bifurcations exist for $\lambda<1/\sqrt{3}$ and do not exist otherwise. At critical value $\lambda<1/\sqrt{3}$ two saddle–node bifurcation points coalesce, thus forming a typical structure of a cusp catastrophe.

It is easy to see from Eq. (31) if only one solution of Eq. (33) exists, it is stable with respect to time scale τ_0. If there are three solutions, two of them are stable (nodes) and one—unstable (saddle). Therefore at time scale τ_0 the phase point will be attracted to one of the nodes. In fact, Eq. (32) defines slow invariant manifold (SIM) of the problem. In the case $\lambda<1/\sqrt{3}$ the fold lines $N_{1,2}=\sqrt{Z^*_{1,2}}$, $\theta(\tau_1)\in(0,2\pi)$, divide stable and unstable branches of the SIM. Fig. 1 demonstrates projection of the two-dimensional (2D) SIM on the plane (N, C), the fold lines correspond to the points of maximum and minimum.

It is well known [25–27] that such structure of the SIM may give rise to relaxation-type oscillations of the system (the hypothetic "jumps" between the stable branches are denoted by arrows at Fig. 1). Still, such motion is possible only if the system can reach the fold lines while moving on the SIM with respect to the slow time scale. Investigation of such motions and necessary conditions for their persistence was done in details in Refs. [22,23,29]. In the present work we only bring the main results of the SMR analysis done by Gendelman et al. [22,23,29]. By now we have described qualitatively the nature of the SMR response. In order to accomplish analysis of the SMR we should also describe the behavior of $\Phi(\tau_1)$ on the SIM (upper and lower branches). For this sake, we consider the ε^1 term of multiple-scale expansion namely the second equation of Eq. (30). We are interested in the behavior of the solution on the stable branches of the SIM $\Phi(\tau_1)=\lim_{\tau_0\to+\infty}\varphi_w(\tau_0,\tau_1)$. Taking the limit $\tau_0\to\infty$ in the second equation of Eq. (30) and taking into account the asymptotic stability of the points of the stable branches with respect to time scale τ_0, one obtains

$$\frac{\partial}{\partial\tau_1}\left[\frac{\lambda\varphi_w}{2}+\frac{\mathrm{i}\varphi_w}{2}-\frac{3\mathrm{i}k_v\left|\varphi_w\right|^2\varphi_w}{8}\right]+\frac{\mathrm{i}(1+2\sigma)}{2}\left[\frac{\lambda\varphi_w}{2}+\frac{\mathrm{i}\varphi_w}{2}-\frac{3\mathrm{i}k_v\left|\varphi_w\right|^2\varphi_w}{8}\right]-\frac{\mathrm{i}\varphi_w\beta}{2}=\frac{A\beta}{2}. \tag{36}$$

Eq. (36) can be written in the more convenient form:

$$\left(\frac{\lambda}{2}+\frac{\mathrm{i}}{2}-\frac{3}{4}\mathrm{i}k_v|\Phi|^2\right)\frac{\mathrm{d}\Phi}{\mathrm{d}\tau_1}-\frac{3}{8}\mathrm{i}k_v\Phi^2\frac{\mathrm{d}\Phi^*}{\mathrm{d}\tau_1}=G,$$
$$G=\frac{-\mathrm{i}\lambda}{4}(1+2\sigma)\Phi+\frac{\sigma}{2}\Phi-\frac{3}{16}k_v(1+2\sigma)|\Phi|^2\Phi+\frac{\mathrm{i}A_1}{4}. \quad (37)$$

System presented in Eq. (37) describes dynamics on the stable branches of the SIM. Results obtained in the present analysis as it was demonstrated in Ref. [29] make it possible to depict the SMR via 1D maps. We will briefly repeat the main results of Ref. [29] and as an example will construct the 1D map depicting the SMR in the limit $\varepsilon\to 0$. We start with the phase portrait constructed for the slow evolved system (37) (Fig. 5).

Observing the phase portrait presented in Fig. 5 one can easily note that there are phase trajectories on either low stable branch or upper one which reach the folds. These trajectories actually allow the existence of SMR. However, it is quite obvious that an existence of these trajectories on each stable branch of SIM cannot guarantee the stability of the SMR. The reason for that is a possibility of the SMR to be attracted to another stable response (e.g. simple periodic) after several jumps from one stable branch to another. In order to track the stability of the SMR response and thus to allow the tools for prediction of its existence 1D maps are assembled. This approach was developed in Ref. [29] and will be applied here. Observing the phase portrait presented at Fig. 5 we can see that there is an interval of θ $[\Theta_1<\theta<\Theta_2]$ for which all the phase trajectories are repelled from the lower fold N_1 ($|\Phi|=N_1$). In the regime of the relaxation oscillations, the phase trajectory jumps from a point of this interval to the upper branch of the SIM, then it moves along the line of the slow flow to the upper fold line, then jumps back to the lower branch and moves to the lower fold line, commencing in one of the points of the interval $[\Theta_1,\Theta_2]$ in order to enable the next jump. Therefore it is natural to consider this regime as mapping of the interval $[\Theta_1,\Theta_2]$ into itself—the regime of the relaxation oscillations will correspond to attractor of this 1D map. Existence of this attractor is therefore necessary and sufficient condition for existence of the SMR for Eq. (27), or, equivalently, Eq. (28), when the mass ratio ε is small enough.

In order to build the relevant mapping, we should consider separately the "slow" and the "fast" parts of the mapping cycle. As for the "slow" parts on the lower and the upper branches of the SIM, we can use Eq. (37) and directly connect the "entrance" and "exit" points. Due to complexity of the equations, this part of the mapping should be accomplished numerically. As for the "fast" parts, the function $\varphi 2$ should be continuous at

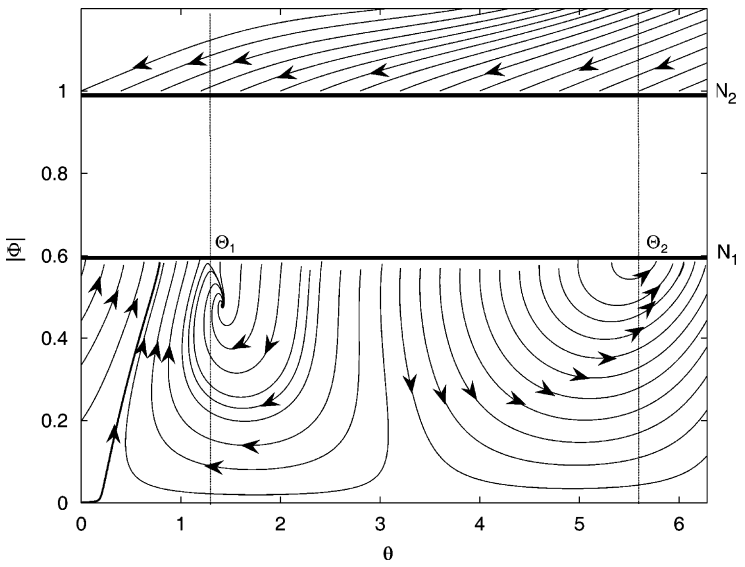

Fig. 5. Phase portrait of the slow invariant manifold (only stable branches of the SIM are shown).

the points of contact between the "fast" and the "slow" parts. Therefore, for "fast" parts of the motion one obtains complex invariant $C(\tau_1)$, defined by Eq. (32). If one knows its value at the point of "start", it is possible co compute N and θ for the point of "finish" unambiguously and thus to complete the mapping. The procedure of numerical integration should be performed twice—for two branches of the SIM. Two invariants should be computed for two "fast" jumps, in order to determine their final points. It should be stressed that

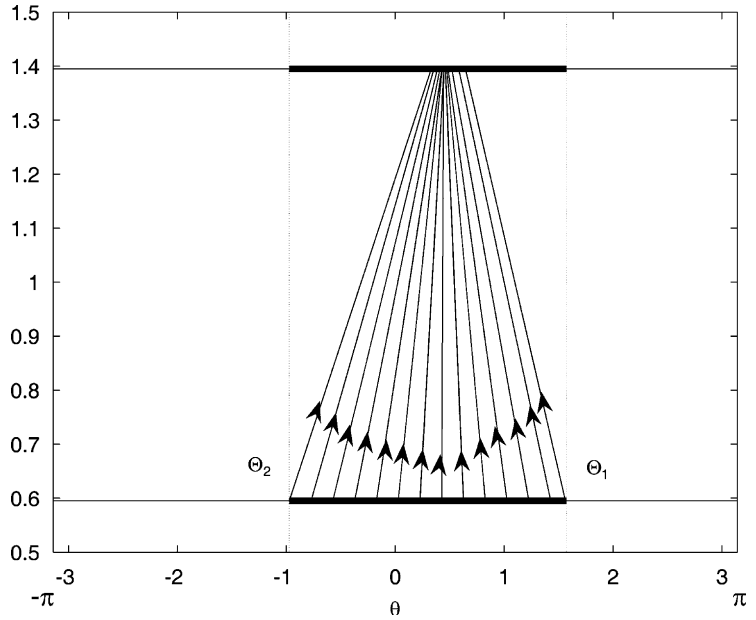

Fig. 6. One-dimensional mapping; $\sigma = -0.5$, $A_1 = 0.6$, $\lambda = 0.2$. Horizontal bold lines refer to the basin of jump $\Theta_1 < \theta < \Theta_2$, arrows denote direction of mapping.

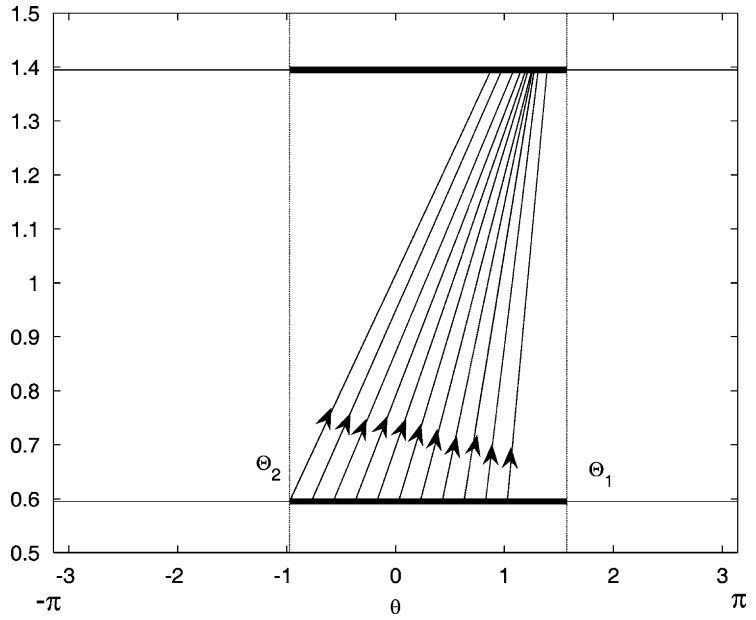

Fig. 7. One-dimensional mapping; $\sigma = -1.45$, $A_1 = 0.6$, $\lambda = 0.2$. Horizontal bold lines refer to the basin of jump $\Theta_1 < \theta < \Theta_2$, arrows denote direction of mapping.

only one computation cycle of the mapping for each point of the initial interval is required. This idea of mapping is close to that used in paper [26] for analysis of chaotic attractors of the relaxation oscillations in the state space of lower dimensionality.

Not every trajectory which starts from the lower fold of the SIM will reach the initial interval since it may be attracted to alternative attractor at the upper or the lower branch of the SIM, if it exists. Of course, only those points which are mapped into the interval can carry sustained relaxation oscillations. The mapping procedure is illustrated in Figs. 6 and 7.

The mapping in Fig. 6 exists for all points of the interval and is obviously contractive; therefore one can expect existence of stable attractor corresponding to the regime of the relaxation oscillations (or SMR). In this case it is single-period cycle originating at a point $\theta \approx 0.51$. By increasing the detuning parameter value (the values of the forcing amplitude and the damping parameters remain the same), one can note the changes that mapping diagram undergoes (Fig. 7). As it comes from the diagram (Fig. 7) all the mapping lines tend to the right and there is also a region on the basin that does not contain any lines. This region relates to the unaccomplished cycles, namely to the phase trajectories which started from the region and have been attracted to the periodic response attractor before they have reached the basin once more.

The mentioned trajectories are not illustrated on the diagram. Thus, the empty regions of basin on the diagrams will be related to the trajectories that do not reach the basin once more. It is clear from Fig. 7 that there is no stable attractor of the SMR and for every initial condition (IC) on the basin the system finally (after sufficient number of cycles) leaves the basin. Consequently, the relaxation oscillations will exist in transient response under certain ICs, but not in the sustained response. Such situation requires presence of alternative attractor.

By now we can conclude that for some increased values of detuning parameter the SMR attractor vanishes. Running with the values of detuning (σ) and for each step performing the mapping one can track the value of σ for which the attractor vanishes. This provides a general tool for determination of the frequency region for the existence of SMR. For the current system, the boundaries of the detuning parameter within which the SMR exists are $\sigma_R = 2.69 > \sigma > \sigma_L = -2.0546$. So, as it was established earlier by direct numerical simulation, the SMR exists in rather small vicinity of the exact 1:1 resonance.

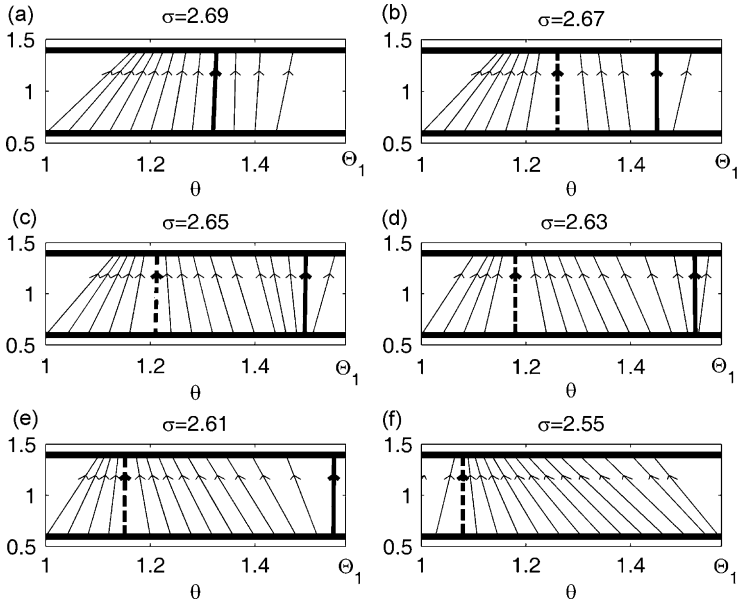

Fig. 8. Sequence of mapping diagrams in the region $(1 < \theta < \Theta_1)$; horizontal bold lines refer to the basin of jump. Stable cycle is marked with bold dashed line and unstable is marked with the bold solid line: (a) $\sigma = 2.69$, (b) $\sigma = 2.67$, (c) $\sigma = 2.65$, (d) $\sigma = 2.63$, (e) $\sigma = 2.61$ and (f) $\sigma = 2.55$.

Our next goal is to investigate the mechanism of "birth" of the limit cycle related to the SMR when the detuning parameter passes its critical value. In Fig. 8 a sequence of mapping diagrams close to upper critical value of the detuning parameter ($\sigma = \sigma_R$) is presented.

For the boundary value ($\sigma = \sigma_R = 2.69$) we can see undistinguishable stable and unstable cycles, separating while the detuning parameter is decreased. This scenario corresponds to simple fold bifurcation of 1D map—creation of stable and unstable fixed points. In the framework of current problem, it corresponds to fold of stable and unstable limit cycles in four-dimensional (4D) state space of the averaged problem (4). This global bifurcation is not related to behavior of fixed points or homoclinic orbits of the problem (the latter are absent in this generic case) and cannot be treated by local analysis. Still, presence of the small parameter related to the mass ratio allows us to reduce the global flow to the 1D nonlinear map and thus to demonstrate this bifurcation in terms of local bifurcation of the map.

Hence, we have depicted the mechanism of creation and annihilation of the stable and unstable cycles about the right boundary (σ_R) of the SMR existence. It is essential to check what happens about the left boundary (σ_L). In order to understand the mechanism by which the loss of the stable cycle occurs we have zoomed the area near the left end of the basin and plotted the diagrams for gradually decreasing values of the detuning parameter near the left boundary (σ_L). The diagrams are presented in Fig. 9.

As one can see from the diagrams of Fig. 9 that for some value of detuning parameter we obtain the creation of the unstable double period cycle right on the left end of the basin. Slightly decreasing the detuning parameter value we can see the movement of the double period cycle from the left end of the basin inside the interior region.

In order to provide an additional illustration of the SMR cycle attractor we have drawn the cycle on the phase portrait plane. These cycles include the fast jumps (from one stable branch of SIM to another) and slow evolution on SIM (Fig. 10).

By now we have accomplished the analytical treatment of the SMR in the vicinity of the first mode. The treatment concerning the SMR in the vicinity of second excited mode is identical to the presented treatment. We will briefly describe the analytical treatment of the SMR in occurrence of the second mode.

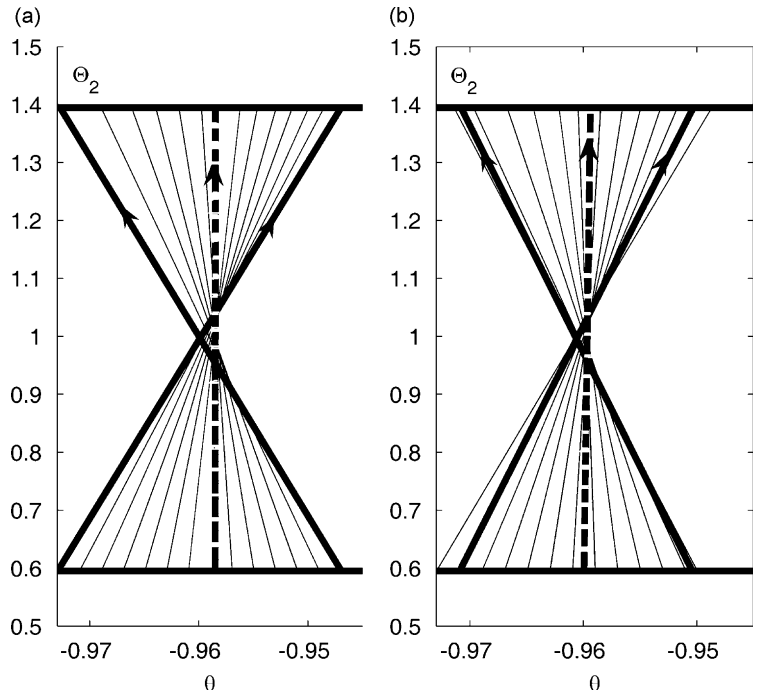

Fig. 9. One-dimensional mapping diagrams: (a) $\sigma = -2.0511$ and (b) $\sigma = -2.052$. The bold line refer to the unstable double period cycle. The bold dashed line refers to the stable one period cycle.

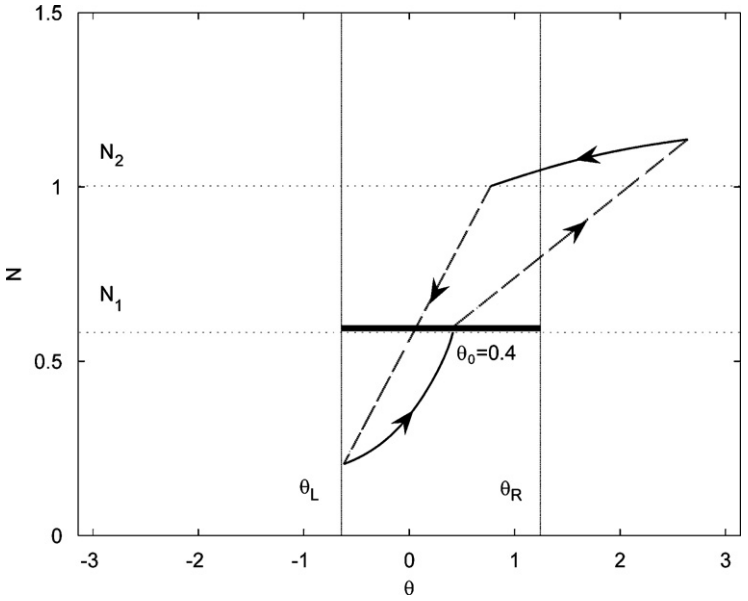

Fig. 10. The entire cycle of SQR; horizontal bold line refers to the initial interval $\Theta_1<\theta<\Theta_2$. Dashed lines refer to the fast jumps and solid line refers to the slow evolution on SIM, $A=0.3$, $\lambda=0.2$, $\sigma=0.5$.

We start with new consideration of the detuning and proper system rescaling. In the case of second mode excitation original system reads

$$\begin{aligned} &x_2''+3x_2=-\varepsilon A_2\cos((3+\varepsilon\sigma)\tau)-\varepsilon k_v(\varepsilon x_1+x_2-v)^3-\varepsilon\lambda(\varepsilon x_1'+\varepsilon x_2'-v'),\\ &x_1''+x_1=\varepsilon A_1\cos((3+\varepsilon\sigma)\tau)-\varepsilon k_v(\varepsilon x_1+\varepsilon x_2-v)^3-\varepsilon\lambda(\varepsilon x_1'+\varepsilon x_2'-v'),\\ &v''+k_v(v-x_1-\varepsilon x_2)^3+\lambda(v'-\varepsilon x_1'-\varepsilon x_2')=0. \end{aligned} \tag{38}$$

By the proper rescaling (as for the case of periodic regimes) Eq. (38) may be reshaped to more convenient form:

$$\begin{aligned} &x_2''+x_2=-\varepsilon A_2\cos((1+\varepsilon\sigma)\tau)-\varepsilon k_v(\varepsilon x_1+x_2-v)^3-\varepsilon\lambda(\varepsilon x_1'+x_2'-v'),\\ &x_1''+\tfrac{1}{3}x_1=\varepsilon A_1\cos((1+\varepsilon\sigma)\tau)-\varepsilon k_v(\varepsilon x_1+x_2-v)^3-\varepsilon\lambda(\varepsilon x_1'+x_2'-v'),\\ &v''+k_v(v-\varepsilon x_1-x_2)^3+\lambda(v'-\varepsilon x_1'-x_2')=0, \end{aligned} \tag{39}$$

where

$$\tilde{A}_2=\frac{A_2}{3},\ \tilde{A}_1=\frac{A_1}{3},\ \tilde{k}_v=\frac{k_v}{3},\ \tilde{\lambda}=\frac{\lambda}{\sqrt{3}},\ \tilde{\sigma}=\frac{\sigma}{\sqrt{3}},\ \tilde{\tau}=\sqrt{3}\tau.$$

Considering only the first and third equations we achieve the system identical to one already treated above (first excited mode).

4. NES tuning

The tuning procedure is based on the analytical treatment results of previous section. As it was shown in papers [24,28] SMR can be much more effective from a point of view of vibration absorption then the simple periodic one in the close vicinity of main resonance (1:1). Thus, the main goal of the tuning procedure is to allow excitement of the SMR in occurrence of each mode for the same attached NES (without changing NES parameters). This situation may be realized in various engineering applications when the linear substructure is subject to harmonic forcing in a wide range of the excitation frequencies. Thus there is a need for a protection

of the system in the whole range of excitation frequency including both dangerous modes. We will demonstrate the tuning procedure concept by considering the following example.

Example 1. Let us consider the following parameters of excitation amplitudes and mass of the nonlinear absorber $A_1 = 1$, $A_2 = 3$, $m = \varepsilon = 0.01$, correspondingly. We need to find a pair of NES parameters (k_v, λ) which allows SMR excitation in the vicinity of each mode of linear subsystem. In order to find such a pair we actually change NES parameters (k_v, λ) with a small step and for each pair we construct the 1D maps in the occurrence of each excited mode. When we finally obtain a certain frequency ranges of SMR existence (stable attractor of the 1D map) about each excited mode we actually satisfied the base requirement of the tuning procedure. Let us imagine that we have performed the described procedure and found a certain pair of $k_v = 1$, $\lambda = 0.2$ parameters which allow excitement of the SMR in the neighborhood of each mode. For this pair we plot frequency-response diagrams for a vicinity of each mode (Fig. 11).

These diagrams consist of periodic regimes amplitudes and frequency range of existence of SMR calculated using 1D map approximation described in the previous section.

Despite the excitement of the SMR in the vicinity of each mode one can note the dangerous situation in the neighborhood of the left bound of the SMR for the first excited mode. Observing the diagram of Fig. 11 for the first excited mode we can see Hopf bifurcation occurs on the lower stable branch slightly before the region of SMR existence (left bound). This bifurcation causes an undesired effect on the system response since the loss of stability by the lower branch will be accompanied by the jump to the upper stable branch which results in large vibration amplitudes. In order to avoid this effect we should attempt to translate Hopf bifurcation of the lower branch into the region of the SMR existence thus assuring continuation from lower stable branch regimes into SMR (without jumps to higher amplitudes). Therefore, increasing damping parameter from $\lambda = 0.2$ to 0.4 we plot the same frequency response diagrams for each excited mode (Fig. 12).

Frequency response diagrams presented at Fig. 12 suggest the continuation between lower stable branch and SMR for both modes. In the next section numerical simulation for the entire frequency range (including both modes) will be carried out for the systems with zero ICs and it will be shown that there are no jumps to the upper branches. It is essential to note that there is also a possibility for the upper stable branch regimes

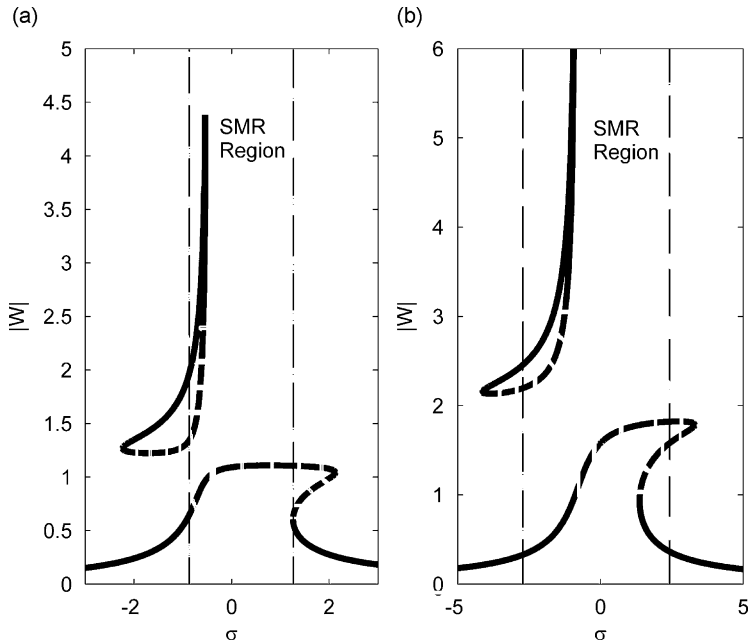

Fig. 11. Frequency response diagrams in occurrence of each excited mode. (a) Vicinity of the first excited mode ($\omega_n = 1$) and (b) vicinity of the second excited mode ($\omega_n = \sqrt{3}$). SMR regions of existence calculated via one-dimensional map are bounded by the dotted lines. Solid bold lines refer to unstable solution whereas thin solid lines refer to the stable ones.

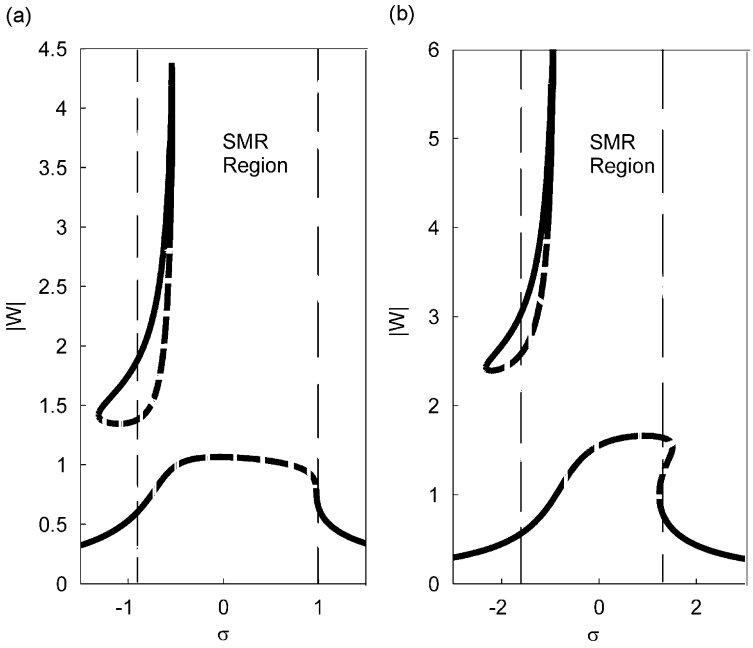

Fig. 12. Frequency response diagrams in occurrence of each excited mode. (a) Vicinity of first excited mode ($\omega_n = 1$) and (b) vicinity of second excited mode ($\omega_n = \sqrt{3}$). SMR regions of existence calculated via one-dimensional map are bounded by the dotted lines. Bold solid lines refer to unstable solution when thin solid lines refer to the stable ones.

excitement by appropriate ICs. However, it will be shown in the following section that those regimes may be excited only by high magnitudes of initial deflections relative to the amplitudes of an external forcing (εA_1, εA_2). In the present work it is also assumed that an excited system does not suffer from strong additional excitations (e.g. impacts, pulses) that are definitely able to push it to the upper branch.

Summarizing the results of an example provided above we have seen that it is not enough to excite the SMR in the vicinity of both system modes, but it is also extremely important to follow after stability of the lower branch of periodic regimes amplitude. As soon as we manage to translate the bifurcation point of the lower branch of periodic response into the region of SMR existence we can enjoy the effectiveness of NES application in a 2dof linear subsystem.

5. Numerical simulations

5.1. Numerical verification of the analytical model

We start numerical verifications of the analytical treatment from frequency response diagrams. Thus, several periodic regimes amplitudes are obtained via numerical integration and are plotted together with analytically derived frequency response curves (Fig. 13).

For the same system parameters ($A_1 = 1$, $A_2 = 3$, $k_v = 1$, $\lambda = 0.4$, $\varepsilon = 0.01$) we have estimated SMR bounds of existence in the vicinity of each mode analytically (using 1D maps) and also via numerical integration. The results of the analytical and numerical estimations are arranged in Table 1.

Verification results demonstrate fairly good agreement between analytic and numeric models.

5.2. NES performance in a wide range of system excitation

In order to study NES performance we plot system response (for zero ICs) vs. frequency of excitation in the entire frequency range, including both modes of the linear subsystem. System response is presented in terms of maximum linear subsystem energy like component ($\max(y_1^2 + y_2^2)$) vs. frequency of excitation (Fig. 13(a)),

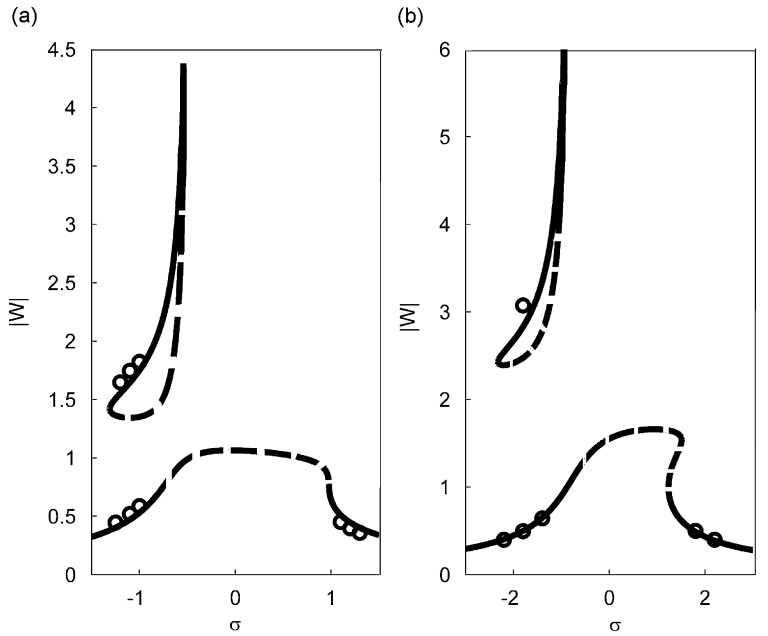

Fig. 13. Numerical verification of frequency response diagrams for each excited mode. (a) Vicinity of first excited mode ($\omega_n = 1$) and (b) vicinity of second excited mode ($\omega_n = \sqrt{3}$). Circles refer to the numerically derived response amplitudes. Solid lines relate to the analytically obtained periodic regimes amplitudes: thin solid line refers to stable response and bold solid line refers to unstable one.

Table 1
Verification of the SMR bounds predicted analytically vs. numerical simulation in the vicinity of each mode

Mode no.	Analytic estimation	Numeric estimation
1	[−0.9:1]	[−0.8:0.9]
2	[−1.6:1.3]	[−1.4:1.2]

maximal deflection of each dof of the linear subsystem (y_1, y_2) vs. frequency of excitation (Fig. 14(b and c)), mean amplitude deflection of each dof of the linear subsystem vs. frequency of excitation (Fig. 14(d and e)). On the same plots we also illustrate the response of an optimally tuned linear absorber. Linear absorber was tuned numerically according to the objective function of the minimal sum of two resonant peaks of the frequency response curve. System parameters for the following simulations are: $A_1 = 1$, $A_2 = 3$, $k_v = 1$, $\lambda = 0.4$, $\varepsilon = 0.01$.

5.3. Excitation zones of preference for SMR

Effectiveness of the SMR has been demonstrated in several resent researches [21,24,28]. It was shown that SMR appears as much more favorable than simple periodic regimes in the vicinity of resonance and for relatively high amplitudes of excitations. This has motivated us to estimate numerically the parametric zones of external amplitudes of excitation for which SMR generated by NES is better than system response with best-tuned linear absorber attached. It should be noted that both linear and nonlinear vibration absorbers are tuned according to the same criteria as in the previous subsection (minimal sum of resonant peaks of the maximal response deflection). Fig. 15 demonstrates dots on a plane of external excitation (A_1, A_2) for which SMR is preferable on the responses of the system coupled to the tuned linear absorber.

Observing the results presented in Fig. 15 one can note that preference of the SMR arises for the relatively high amplitudes of excitation. This result is not surprising since it comes from the analytical model the upper branch of the SIM does not depend on the amplitude of excitation. Therefore for some low amplitudes of

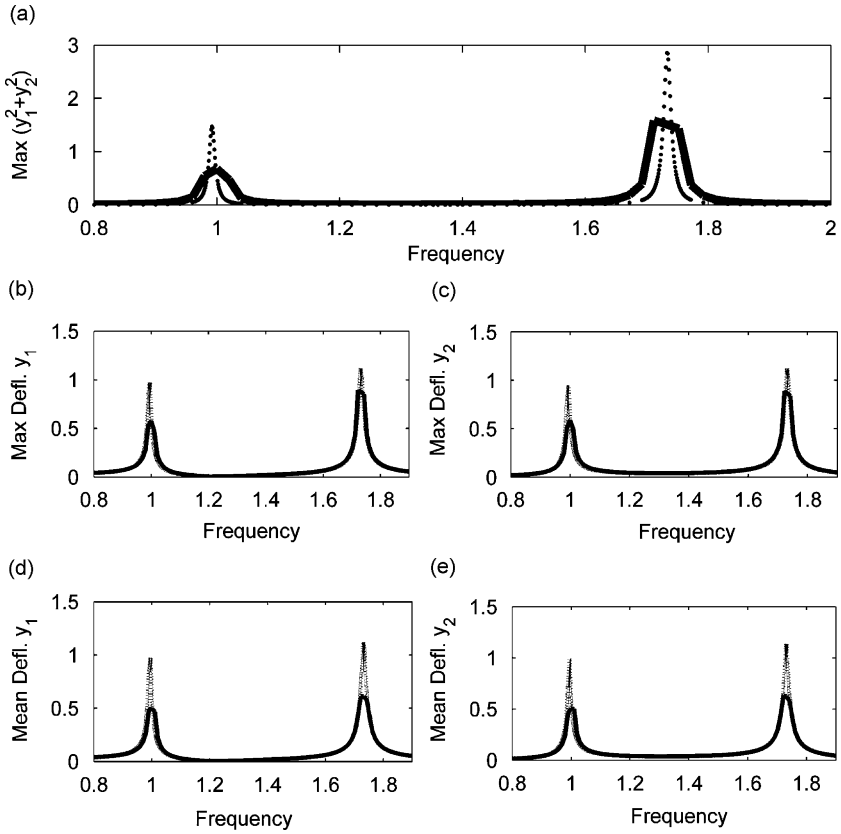

Fig. 14. (a) Linear subsystem energy like response vs. frequency of excitation; bold line refers to the system response with NES attached when dotted line refers to the system response with tuned linear absorber attached. (b and c) Maximal amplitude deflection of linear subsystem dofs (y_1,y_2); bold line refers to the response with NES attached wheras dotted line refers to the response with tuned linear absorber attached. (d and e) Mean amplitude deflection of linear subsystem dofs (y_1,y_2); bold line refers to the system response with NES attached whereas dotted line refers to the system response with tuned linear absorber attached.

excitation SMR may be already excited however system response will be rather high comparing with the case of linear absorber application. In the case of high amplitudes of excitation system response with linear absorber attached will overcome the SMR response. This is due to the fact that SMR is weakly affected by the growth of the amplitude of excitation contrary to the case of linear absorber application.

5.4. Numeric estimation of the system robustness

Robustness of the response regimes in a linear oscillator with the NES attached to variation of the parameters has been extensively studied in Refs. [22,24], but the issue of variations of the IC has not been addressed. Still, this issue is crucial: if one succeeds to establish that for well-defined range of the IC the system response will remain on "favorable" branch of the response curve, then the situation may be considered as "acceptable' from the viewpoint of the vibration absorption despite presence of the other, less favorable responses. In order to demonstrate the robustness of the periodic response regime related to the lower stable branch of the frequency response curves and SMR we have performed numerical integration for the random set of ICs. Thus, randomly picking 300 triples of initial deflections (x_{10}, x_{20}, v_0) in the following range ($-0.5 \leqslant (x_{10}, x_{20}, v_0) \leqslant 0.5$), original Eq. (7) was integrated numerically in the vicinity of each mode. Randomly selected values of ICs for which Eq. (7) was integrated are presented in Fig. 16.

Each simulation was done for the random set of initial deflections data (initial velocities are set to zero) shown in Fig. 16. Two frequencies of excitation were picked for each mode. The first selected frequency refers to the region of two stable periodic regimes coexistence not including SMR. The second one refers to the

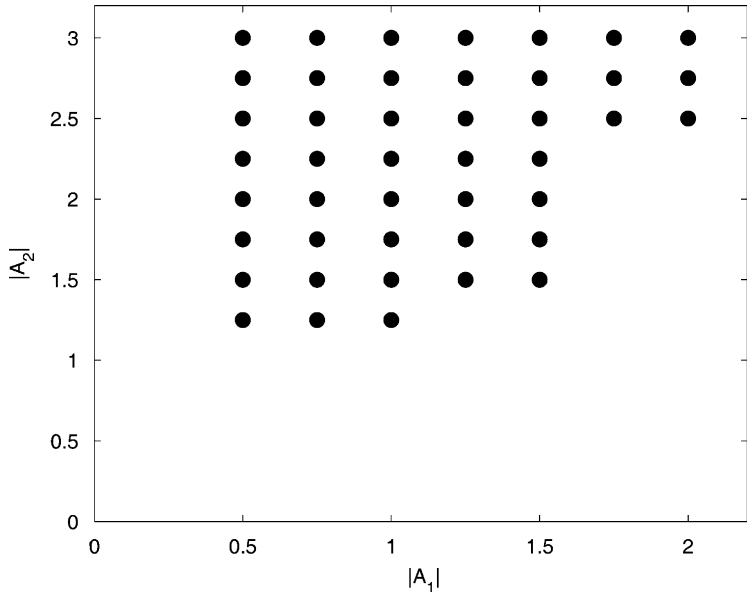

Fig. 15. External excitation plane, dots are related to those excitation amplitudes for which SMR is preferable on the response of system coupled to the tuned linear absorber.

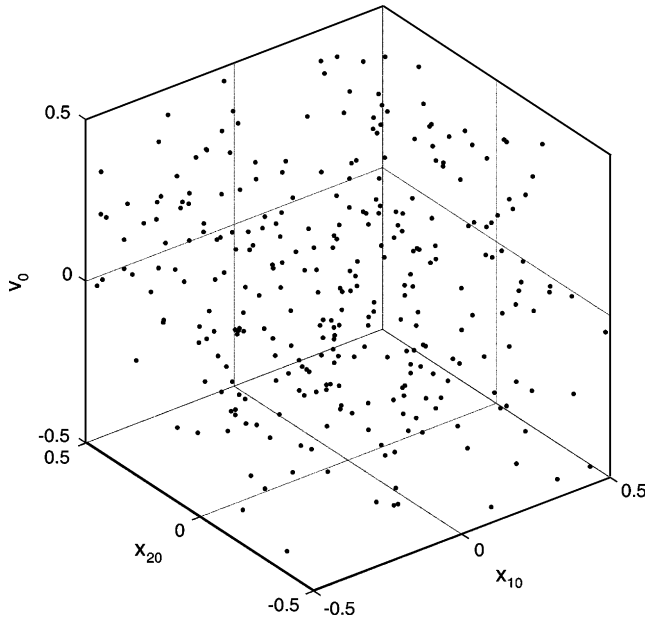

Fig. 16. Random data of the initial deflections in the range $(-0.5 \leqslant (x_{10}, x_{20}, v_0) \leqslant 0.5)$.

region of coexistence of SMR together with stable periodic response related to the upper branch of frequency response curve. Frequencies of excitation are as follows:

$$\text{First mode:} \quad \omega = 1 + \varepsilon\sigma \quad (\sigma = -1,\ -0.8),$$
$$\text{Second mode:} \quad \omega = \sqrt{3} + \varepsilon\sigma \quad (\sigma = -1.5,\ -1).$$

System parameters: $A_1 = 1$, $A_2 = 3$, $\varepsilon = 0.01$, $\lambda = 0.4$, $k_v = 1$.

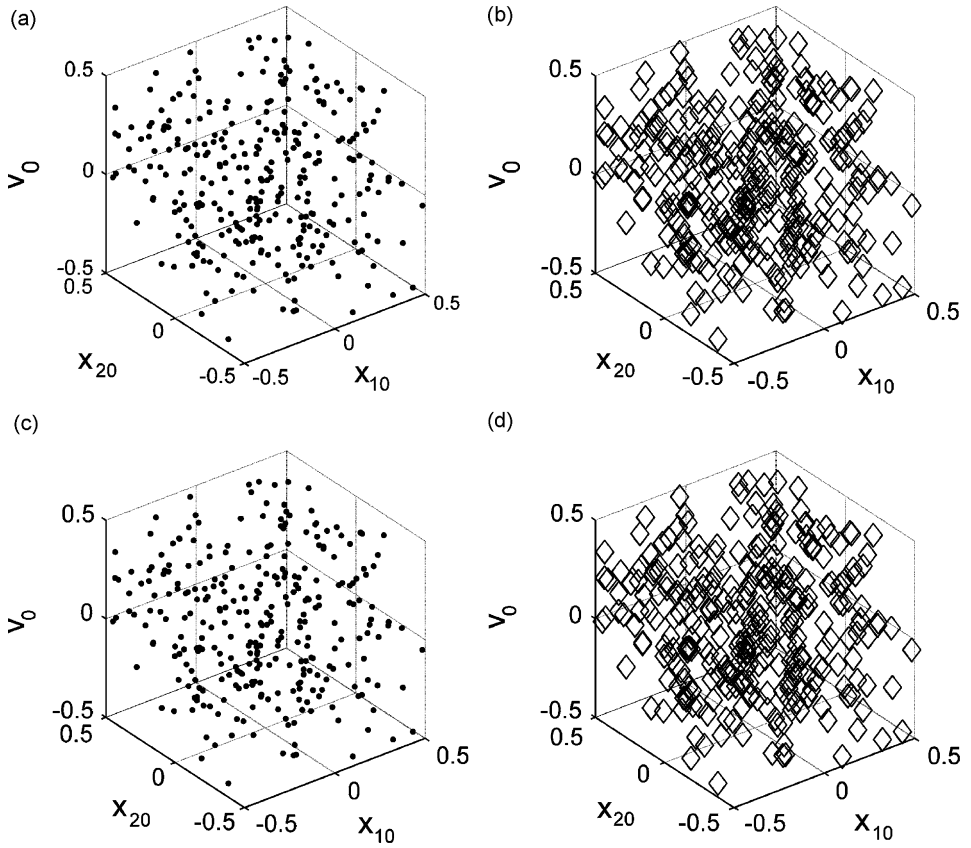

Fig. 17. Initial conditions data for several frequencies of excitation: (a) vicinity of the first mode ($\omega_n = 1$, $\sigma = -1$), (b) vicinity of the first mode ($\omega_n = 1$, $\sigma = -0.8$), (c) vicinity of the second mode ($\omega_n = \sqrt{3}$, $\sigma = -1.5$), (a) vicinity of the second mode ($\omega_n = \sqrt{3}$, $\sigma = -1.2$). Dots are related to the periodic r response regime of the lower stable branch and diamonds are related to the SMR.

The results of the simulations are illustrated in Fig. 17. Each point of the random set of ICs is marked with respect to the type of the steady-state response regime obtained by numerical integration started from this particular IC. Thus 'diamond' marker refers to SMR, 'dot' marker refers to the periodic regime of the lower stable branch and 'circle' marker refers to the one of the upper stable branch.

It is clear from the results presented at in Fig. 17 that for the frequency of excitation in zone of the coexistence of two periodic regimes for both modes all the trajectories which correspond to the brought above ICs are attracted to the lower stable branch of periodic response regime. For the frequency of excitation in zone of the coexistence of SMR and periodic responses for both modes, all trajectories corresponding to the same set of the ICs are attracted to the SMR. Obtained results provide additional confirmation of the robustness of the periodic regime related to the lower stable branch and SMR in the vicinity of zero ICs. It is essential to note that the range of initial deflections is of magnitude which is much higher than the amplitude of the external excitation.

6. Conclusions

Present work extends the developed earlier [22–24,29,30] analytic methods for description of simple periodic and strongly modulated regime to 3dof harmonically excited system. Considered system is comprised of harmonically forced 2dof linear subsystem (primary system) and essentially nonlinear attachment. It is shown that analytical methods developed in Ref. [29] for the description of periodic regimes and SMR may be successfully applied to the described 3dof system in case when modal frequencies are remote and incommensurate. Derived analytical model is used for estimation of system responses and guidelines for the

nonlinear absorber tuning are formulated. Numerical verification of the analytical model is performed and fairly good agreement is observed.

As it comes from numerical simulations in some cases of high amplitudes of excitation nonlinear absorber may effectively absorb energy from the primary linear subsystem for both excited system modes. In these cases nonlinear absorber appears to be much more favorable than linear one. Thus summarizing the drawbacks of the essentially nonlinear vibration absorber we note its inefficiency for the low amplitudes of excitation and an existence of additional branch of periodic regimes with relatively high magnitude. However as it was demonstrated in the previous section the last drawback may be minimized by proper NES design and these regimes are not excited for the certain range of ICs. The magnitude of this range is much bigger than the amplitudes of an external excitation and thus provides a fairly good approximation to the real life applications. It should be mentioned that the quasi-periodic notions of the absorber, which frequently are associated with undesirable large-amplitude vibrations, in this particular system turn out to be favorable for vibration absorption.

Acknowledgment

The authors are grateful to Israel Science Foundation (Grant 486/05) for financial support.

References

[1] H. Frahm, Device for damping vibrations of bodies, US Patent 989,958, 1911.
[2] J.P. Den Hartog, *Mechanical Vibrations*, fourth ed., McGraw-Hill Book Company, New York, 1956.
[3] J. Ormondroyd, J.P. Den Hartog, The theory of the dynamic vibration absorber, *Transactions of the American Society of Mechanical Engineers* 50 (1928) A9–A22.
[4] M.N.S. Hadi, Y. Arfiadi, Optimum design of absorber for MD structures, *Journal of Structural Engineering* 124 (1998) 1272–1280.
[5] M.P. Singh, L.M. Moreschi, Optimal placement of dampers for passive response control, *Earthquake Engineering and Structural Dynamics* 31 (2002) 955–976.
[6] Mehmet Bulent Ozer, Thomas J. Royston, Extending Den Hartog's vibration absorbertechnique to multi-degree-of-freedom systems, *Journal of Vibration and Acoustics* 127 (4) (2004) 341–350.
[7] R.E. Roberson, Synthesis of a nonlinear dynamic vibration absorber, *Journal of the Franklin Institute* 254 (1952) 205–220.
[8] J. Shaw, S.W. Shaw, A.G. Haddow, On the response of the nonlinear vibration absorber, *International Journal of Non-Linear Mechanics* 24 (1989) 281–293.
[9] H.J. Rice, J.R. McCraith, Practical non-linear vibration absorber design, *Journal of Sound and Vibration* 116 (3) (1987) 545–559.
[10] I.N. Jordanov, I.B. Cheshankov, Optimal design of linear and nonlinear dynamic vibration absorbers, *Journal of Sound and Vibration* 123 (1988) 157–170.
[11] S. Natsiavas, Steady state oscillations and stability of non-linear dynamic vibration absorbers, *Journal of Sound and Vibration* 156 (2) (1992) 227–245.
[12] O.V. Gendelman, Transition of energy to nonlinear localized mode in highly asymmetric system of nonlinear oscillators, *Nonlinear Dynamics* 25 (2001) 237–253.
[13] O.V. Gendelman, A.F. Vakakis, L.I. Manevitch, R. McCloskey, Energy pumping in nonlinear mechanical oscillators I: dynamics of the underlying Hamiltonian system, *Journal of Applied Mechanics* 68 (1) (2001) 34–41.
[14] A.F. Vakakis, O.V. Gendelman, Energy pumping in nonlinear mechanical oscillators II: resonance capture, *Journal of Applied Mechanics* 68 (1) (2001) 42–48.
[15] A.F. Vakakis, Inducing passive nonlinear energy sinks in linear vibrating systems, *Journal of Vibration and Acoustics* 123 (3) (2001) 324–332.
[16] A.F. Vakakis, L.I. Manevitch, O. Gendelman, L. Bergman, Dynamics of linear discrete systems connected to local essentially nonlinear attachments, *Journal of Sound and Vibration* 264 (2003) 559–577.
[17] O.V. Gendelman, Bifurcations of nonlinear normal modes of linear oscillator with strongly nonlinear damped attachment, *Nonlinear Dynamics* 37 (2) (2004) 115–128.
[18] S.W. Shaw, C. Pierre, Normal modes for nonlinear vibratory systems, *Journal of Sound and Vibration* 164 (1993) 85–124.
[19] A.F. Vakakis, L.I. Manevitch, Yu.V. Mikhlin, V.N. Pilipchuk, A. Zevin, *Normal Modes and Localization in Nonlinear Systems*, Wiley Interscience, New York, 1996.
[20] X. Jang, M. McFarland, L.A. Bergman, A.F. Vakakis, Steady state passive nonlinearenergy pumping in coupled oscillators: theoretical and experimental results, *Nonlinear Dynamics* 33 (2003) 7–102.
[21] O.V. Gendelman, E. Gourdon, C.H. Lamarque, Quasiperiodic energy pumping in coupled oscillators under periodic forcing, *Journal of Sound and Vibration* 294 (2006) 651–662.

[22] O.V. Gendelman, Y. Starosvetsky, Quasiperiodic response regimes of linear oscillator coupled to nonlinear energy sink under periodic forcing, *Journal of Applied Mechanics* 74 (2006) 325–331.
[23] O.V. Gendeman, Y. Starosvetsky, M. Feldman, Attractors of harmonically forced linear oscillator with attached nonlinear energy sink I: description of response regimes, online first, *Nonlinear Dynamics* (2007), doi:10.1023/A:1012967003477.
[24] Y. Starosvetsky, O.V. Gendelman, Attractors of harmonically forced linear oscillator with attached nonlinear energy sink II: optimization of a Nonlinear vibration absorber, online first, *Nonlinear Dynamics* (2007), doi:10.1007/s11071-006-9168-z.
[25] V.I. Arnold, V.S. Afrajmovich, Y.S. Il'yashenko, L.P. Shil'nikov, *Dynamical Systems V. Encyclopedia of Mathematical Sciences*, Springer, Berlin, 1994.
[26] J. Guckenheimer, M. Wechselberger, L.-S. Young, Chaotic attractors of relaxation oscillators, *Nonlinearity* 19 (2006) 701–720.
[27] J. Guckenheimer, K. Hoffman, W. Weckesser, Bifurcations of relaxation oscillations near folded saddles, *International Journal of Bifurcations and Chaos* 15 (11) (2005) 3411–3421.
[28] E. Gourdon, N.A. Alexander, C.A. Taylor, C.H. Lamarque, S. Pernot, Nonlinear energy pumping under transient forcing with strongly nonlinear coupling: theoretical and experimental results, *Journal of Sound and Vibration* 300 (2007) 522–551.
[29] Y. Starosvetsky, O.V. Gendelman, Strongly modulated response in forced 2DOF oscillatory system with essential mass and potential asymmetry, *Physica D* (2007), submitted for publication.
[30] Y. Starosvetsky, O.V. Gendelman, Extensive study of periodic regimes of linear oscillator coupled to nonlinear energy sink under periodic forcing—account of detuning, *Proceedings of ASME DETC-2007, paper DETC2007-34222*, 2007.
[31] Y. Lee, G. Kerschen, D. McFarland, W. Hill, C. Nichkawde, T. Strganac, L. Bergman, A. Vakakis, Suppressing aeroelastic instability using broadband passive targeted energy transfers, part 2: experiments, *AIAA Journal* 45 (2007) 2391–2400.
[32] B. Cochelin, P. Herzog, P.-O. Mattei, Experimental evidence of energy pumping in acoustics, *Comptes Rendus Mechanique* 334 (2006) 639–644.